Physicochemical Investigation of Pulsed Laser Deposited Carbonated Hydroxyapatite Films on Titanium

Julietta V. Rau,*,† Amanda Generosi,† Sara Laureti,‡ Vladimir S. Komlev,§ Daniela Ferro,|| Stella Nunziante Cesaro,|| Barbara Paci,† Valerio Rossi Albertini,† Elisabetta Agostinelli,‡ and Sergey M. Barinov§

Istituto di Struttura della Materia, Consiglio Nazionale delle Ricerche, Via del Fosso del Cavaliere 100, 00133 Rome, Italy, Istituto di Struttura della Materia, Consiglio Nazionale delle Ricerche, Via Salaria km 29.300, 00016 Monterotondo Scalo (RM), Italy, A. A. Baikov Institute of Metallurgy and Materials Science, Russian Academy of Sciences, Leninsky prospect 49, 119991 Moscow, Russia, and Istituto per lo Studio dei Materiali Nanostrutturati, Consiglio Nazionale delle Ricerche, Piazzale Aldo Moro 5, 00185 Rome, Italy

ABSTRACT Carbonated hydroxyapatite (CHA)-coated titanium can find wide applications as bone substitute implant in bone and dental surgery and orthopedics, promoting osseointegration with a host bone and ensuring biocompatibility and bioactivity. In this work, carbonated hydroxyapatite films were prepared on titanium substrates by pulsed laser deposition at different substrate temperatures ranging from 30 to 750 °C. The properties of films were investigated by scanning electron microscopy, atomic force microscopy, energy-dispersive X-ray diffraction, and Fourier transform infrared spectroscopy. Vickers microhardness measurements of the composite film−substrate systems were performed, and the intrinsic hardness of films was separated from the composite hardness using a "law-of-mixtures" approach and taking into account the indentation size effect. The prepared CHA films are nearly stoichiometric with a Ca/P atomic ratio of 2.0−2.2. The films deposited in the 30−500 °C temperature range are about 9 μm thick, amorphous, having an average roughness of 60 nm. At higher temperature, 700−750 °C, the films are about 4 μm thick, show a finer surface morphology and an average roughness of 20 nm. At 750 °C the films are amorphous, whereas at 700 °C they are crystalline and textured along the (202) and (212) directions. The intrinsic hardness of the films increased with an increase in substrate temperature, being as low as 5 GPa at 30 °C and reaching a high value of 28 GPa at 700 °C. The rich information gained by the joint use of the mentioned techniques allowed a comprehensive characterization of this system.

KEYWORDS: carbonate hydroxyapatite • films • pulsed laser deposition • characterization • hardness

1. INTRODUCTION

Titanium and titanium-based alloys are widely used in clinical practice as implant orthopedic materials (1−5). However, titanium is a relatively soft material, which can oxidize under the pH conditions of human body fluids that surround orthopedic and tooth implants (1, 6). Modification of titanium surface by various coatings, providing biocompatibility, protection against oxidation, enhanced corrosion resistance, and hardness, and therefore, superior wear resistance of the implant could be performed. Calcium phosphates are widely used for implant coatings in biomedical applications (7, 8). A calcium phosphate belonging to the group of biocompatible and bioactive ceramics, hydroxyapatite, is the main constituent of the mineral component of the natural bone and teeth. However, biological apatite is nonstoichiometric and contains between 2.3 and 8.0 wt % carbonate (9, 10). Therefore, the key target of biomaterials research is the preparation of synthetic bone-substitute ceramics that closely resembles the chemical composition of hard tissue. Carbonate-substituted hydroxyapatite is characterized by increased solubility and improved bioactivity compared to hydroxyapatite (HA) (11 −15).

A number of methods have been reported in the literature for calcium phosphate coatings deposition, among them plasma-spraying (16, 17), sol−gel technology (18), ion-beam deposition (19), molecular precursor method (20), and pulsed laser deposition (21−28). In this study, we applied the latter versatile technique, referred to as PLD, which exhibits some advantages such as preservation of the stoichiometry of target material; control of the adherence, crystallinity, and surface roughness; reduced pollution of the deposited films; possibility of ablation from various target materials; and fabrication of coatings on any substrate material, e.g., metal, ceramic, and plastic.

The aim of the present work was to systematically study the structural, chemical and morphological quality of pulsed laser deposited CHA films on titanium substrates as a function of the deposition temperature. This information is

* Corresponding author. Tel: 39-06-4993 4124. Fax: 39-06-4993 4153. E-mail: giulietta.rau@ism.cnr.it.

Received for review May 26, 2009 and accepted July 7, 2009

† Istituto di Struttura della Materia, Consiglio Nazionale delle Ricerche.

‡ Istituto di Struttura della Materia, Consiglio Nazionale delle Ricerche.

§ A. A. Baikov Institute of Metallurgy and Materials Science, Russian Academy of Sciences.

|| Istituto per lo Studio dei Materiali Nanostrutturati, Consiglio Nazionale delle Ricerche.

DOI: 10.1021/am900356e

necessary because biological behavior of coated metallic implants strongly depends on the coating morphology and microstructure. The films morphology, along with their surface topography, were investigated by the scanning electron microscopy (SEM) coupled with a system for microanalysis (energy-dispersive x-ray spectroscopy (EDXRS)) and the atomic force microscopy (AFM). Conversely, the samples microstructure was studied by the energy-dispersive X-ray diffraction (EDXRD) method. In addition, the molecular structure of the films was investigated by Fourier transform infrared spectroscopy (FTIR). Finally, for the mechanical properties characterization, Vickers microhardness measurements of CHA films on titanium substrates were carried out, and the intrinsic hardness of the films was evaluated using the "law-of mixtures" approach.

2. EXPERIMENTAL SECTION

2.1.Materials. Carbonate-substituted hydroxyapatite was synthesized according to reaction 1 between calcium oxide, ammonium hydrogen phosphate, and ammonium carbonate

$$10CaO + 6(NH_4)_2HPO_4 + (NH_4)_2CO_3 + 4H_2O \rightarrow Ca_{10}(PO_4)_{6-y}CO_3(OH)_{2-z} + 14NH_4OH; 3y + z = 2 \quad (1)$$

Analytical-grade initial reagents were mixed in equimolar ratio (28 g of CaO, 39.6 g of $(NH_4)_2HPO_4$, and 4.8 g of $(NH_4)_2CO_3$) in a planetary ball mill for 30 min. After that, 300 mL of H_2O was added to the mixture, and the mixing procedure was continued for another 30 min. The mixture was then placed in a domestic microwave oven (Electronica, 2.45 GHz, 630W) for 40 min. The reaction product, white powder, was then subjected to the heat treatment at 300 °C in an air atmosphere furnace.

To reduce the sintering temperature and prevent the CHA decomposition, we added up to 8 wt % alkaline/alkaline-earth carbonates to the CHA powder prior to disk-target preparation. CHA disk-target of 20 mm diameter and 4 mm thickness was uniaxially pressed at 100 MPa pressure at room temperature and further sintered at 750 °C for 1 h in the air.

Pure titanium substrates were sandblasted by a 60-grid SiC abrasive to provide surface roughness of approximately 7 nm.

2.2. Methods. 2.2.1. ***Chemical Analysis.*** Chemical analysis of carbon content was performed on the CHA targets according to the Russian Standard GOST procedure, measuring the volume of gas, produced by the reaction between sample and hydrochloric acid. The carbon content in the prepared target was 1.6 ± 0.2 wt %, which corresponds to 7.6 wt % carbonate groups. The Ca/P atomic ratio was 1.74. It is higher than that in stoichiometric HA (1.67), which points to the partial replacement of phosphate groups by carbonate groups.

2.2.2. ***Pulsed Laser Deposition.*** Films were deposited on the treated Ti substrates at different substrate temperatures (namely: 30, 200, 400, 500, 700, and 750 °C) in a high-vacuum PLD chamber. Depositions were performed by focusing a pulsed KrF Lambda Physik excimer laser (λ = 248 nm, pulse duration = 17 ns) on the sintered CHA rotating target, the rotation being necessary to ensure homogeneous ablation of the material. The spot energy fluence was 2 J/cm^2, with a pulse repetition rate of 5 Hz; for a total of 4500 pulses, the total deposition time was 15 min. The laser beam was oriented with an inclination angle of 45° with respect to the target, whereas substrate and target were assembled in a frontal geometry at 4 cm of reciprocal distance. The PLD chamber was evacuated down to a base pressure of 1×10^{-6} mbar prior to the film deposition; then, depositions were performed at 5×10^{-4} mbar in a controlled dynamic pressure produced by N_2 gas flow, introduced directly into the chamber through a needle valve.

2.2.3. ***Scanning Electron Microscopy Analysis.*** Scanning electron microscopy (a LEO 1450 Variable Pressure apparatus), working in secondary and backscattered electron modes, was used for morphological studies of the CHA films. The SEM apparatus is coupled with a system for microanalysis EDXRS INCA 300 that allows executing qualitative/quantitative analysis of the elements starting from atomic number 5 (Boron) with the sensitivity limit of about 0.2%. The resolution of the apparatus in vacuum conditions is about 4 nm. Both plane and cross-section view images of the film samples were obtained, the latter being necessary for thickness measurements.

2.2.4. ***Atomic Force Microscopy Analysis.*** The AFM measurements were performed in the noncontact mode using a noncommercial air-operating atomic force microscope (29). Several portions of the sample surfaces were topographically/phase-shift reconstructed in order to evaluate the morphological/chemical homogeneity of the depositions. Afterward, the high definition topographic images (3 μm × 3 μm and 5 μm × 5 μm, 800 points/line) were collected from representative portions of the films in order to quantitatively evaluate the surface texture and roughness.

2.2.5. ***Energy-Dispersive X-ray Diffraction Analysis.*** The Energy Dispersive X-ray Diffraction measurements were performed by a noncommercial instrument described in detail elsewhere (30, 31). The same apparatus was used to perform the rocking curve (RC) analysis (31) of the samples. The EDXRD technique provides the simultaneous measure of all the RCs of the most intense Bragg reflections for both the film and the substrate. To fit the peaks of each pattern in order to calculate its intensity as a function of the asymmetry parameter α, the sum of a Gaussian and a linear function are used: the Gaussian component takes into account the convolution of the Bragg peak with the diffractometer transport function, whereas the linear one, the contribution of an almost flat background and of the smooth Compton profile. The Gaussian integral is proportional to the peak coherently scattered intensity, which is used to calculate the rocking curve, while its maximum indicates the position of the Bragg peak, required to get the interplanar spacing.

Because the X-ray diffraction provides information about the lattice structure in the direction of the momentum transfer, the measurement of the rocking curves of the film perpendicular to the *c*-direction allows for evaluating both its degree of epitaxy and a possible misalignment of the average orientation of its domains with respect to the substrate domains.

2.2.6. ***Fourier Transform Infrared Spectroscopy Analysis.*** CHA films deposited on Ti substrates were investigated by Fourier transform infrared spectroscopy using a Bruker Hyperion 3000 microscope connected to a Bruker Equinox 55 interferometer. A KBr beamsplitter, a Globar source and a mercury−cadmium-telluride detector were used with the microscope working in reflection mode at a spectral resolution of 2 cm^{-1}. Both sample and reference spectra were collected averaging at least 200 interferograms. The Ti substrate was used for measuring the reference spectrum. Transmittance spectra were calculated, and baseline correction was applied by OPUS 6.5 software. Several FTIR spectra were collected randomly upon each film and gave reproducible results.

2.2.7. ***Vickers Microhardness Measurements.*** The microhardness measurements were performed by means of a Leica VMHT apparatus (Leica GmbH, Germany) equipped with a standard Vickers pyramidal indenter (square-based diamond pyramid of 136° face angle). The loading and unloading speed was 5×10^{-6} m/s, and the time under the peak load was 15 s. The hardness of the Ti substrate, bulk target, and films was measured according to the procedure described in detailed in our previous works (32, 33).

For film samples, the measured hardness was that of the film/substrate composite system. To separate the composite hardness of the film/substrate system (H_c) into its components, film (H_f) and substrate (H_s), we applied a Jönsson and Hogmark model based on area "law-of-mixtures" approach (34), taking into account the indentation size effect (35). In this case, composite hardness H_c is expressed as

$$H_c = H_{s0} + [B_s + 2ct(H_{f0} - H_{s0})]/D \quad (2)$$

where $c \cong 0.5$ for a brittle hard film on a more ductile substrate (34); H_{s0} and H_{f0} are the intrinsic hardness of substrate and film, respectively; t is film thickness; D is the indentation diagonal, and B_s is the coefficient, which can be deduced from substrate hardness measurements.

To evaluate H_{s0} and B_s values, we first measured the hardness of the Ti substrate. The relation between the measured substrate hardness, H_s, and the reciprocal length of the indentation imprints is expressed by the following equation (36)

$$H_s = H_{s0} + B_s/D \quad (3)$$

The values obtained for the titanium substrate, H_{s0} and the B_s coefficient, are equal to 1.8 ± 0.1 GPa and $(5.4 \pm 1.0) \times 10^{-6}$ GPa m, respectively.

To calculate the intrinsic hardness of films, we paid special attention to correctly choosing the indentation depths, $d = D/7$ (for Vickers pyramidal indenter), in the range where the applied model is valid. The $d/t = D/7t$ range for the CHA films deposited on Ti substrates was (0.1−3.4), perfectly in the range of the substrate-dominated mixed region, where the film is fractured conforming to the plastically deforming substrate (37). In this d/t range, the results obtained using the Jönsson and Hogmark model have been demonstrated to coincide quite well with estimations resulting from more complicated models (37, 38).

For hardness measurements on both the CHA bulk target and the CHA film/Ti substrate system, indentations were made applying 7 loads ranging from 0.2 up to 9.8 N. For each sample, approximately 10−15 indentations were made at each load.

3. RESULTS AND DISCUSSION

SEM analysis was performed to evaluate the morphology of the prepared films. Plane view images of CHA films on Ti substrates at different magnifications are shown in Figures 1 and 2. As one can see, the surfaces of all the films prepared at various substrate temperatures are uniform and dense, composed of grains and droplets up to micrometer size. The films deposited in the range of 30−500 °C are characterized by very similar morphology (images a and b in Figure 1), whereas the increase in substrate temperature up to 700−750 °C leads to significant morphological changes: the film surface becomes more compact and finely granulated (images a and b in Figure 2).

Cross-section images for film's thickness evaluation were obtained by tilting the samples at 45°. The thickness of films deposited at different substrate temperature are summarized in Table 1.

As the Ca/P ratio is one of the important characteristics of calcium phosphates, EDXRS was performed for qualitative chemical analysis of the films. The obtained results indicate a Ca/P atomic ratio of 1.77 for the CHA target, this value being in agreement with that obtained by chemical analysis

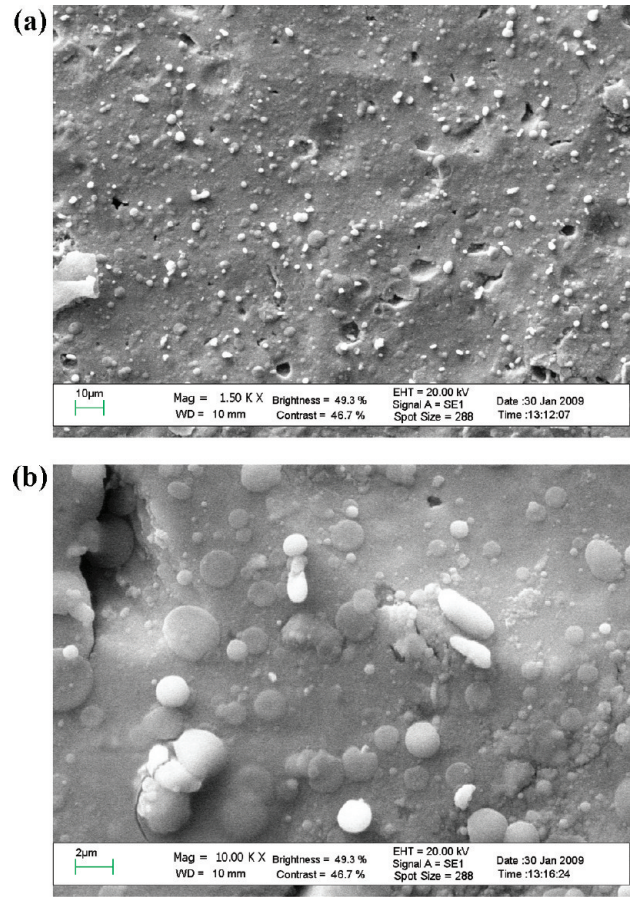

FIGURE 1. SEM micrographs of CHA films deposited on Ti substrates at 500 °C at (a) 1500 and (b) 10 000 magnification.

(1.74). For the films, the Ca/P atomic ratio is 1.81 for those deposited at 30 °C, 2.10 for films deposited in the range of 200−700 °C, and 2.20 for films deposited at 750 °C. The increased Ca/P ratio of films with respect to the target is probably due to a partial loss of the lighter element, phosphorus, with respect to calcium during laser ablation, an effect becoming more evident with the increase in deposition temperature.

The topography of the film surface was examined by AFM. Several images of each film were collected. The films deposited in the temperature range of 30−500 °C show a quite similar surface texture. In Figure 3, image a is representative of such morphology, characterized by large domains, 500−600 nm of average height, 1−3 μm of average lateral dimension, rms ≈ 62 nm of average roughness. It is worth noticing that a large surface roughness does not represent a problem for coated metallic implants in biomedical applications, because roughness usually ensures a better osteointegration, as compared to smoother implants (39).

In the case of film deposited at 700 °C, the AFM images are remarkably different, compared to those of films deposited at lower temperatures, as shown in Figure 3b. Several images were collected from different portions of the sample and its average roughness appeared to be always much lower (rms = 18 nm, see Figure 4), indicating that a higher temperature favored growth of a smoother and a more

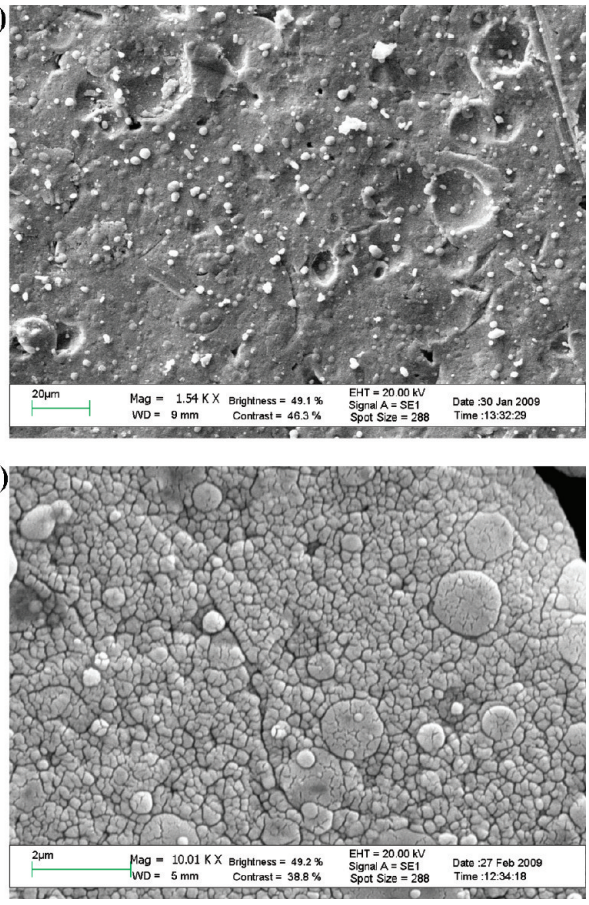

FIGURE 2. SEM micrographs of CHA films deposited on Ti substrates at 700 °C at (a) 1500 and (b) 10 000 magnification.

Table 1. Thickness and Hardness of CHA Films on Ti Substrates Deposited at Different Temperatures

deposition T (°C)	thickness (μm)	hardness (GPa)
30	10.0 ± 1.0	5 ± 1
200	9.0 ± 1.0	8 ± 2
400	8.0 ± 1.0	8 ± 2
500	8.0 ± 1.0	6 ± 1
700	3.8 ± 0.4	28 ± 3
750	3.8 ± 0.4	21 ± 3

homogeneous surface. Furthermore, along with the micrometric size domains, which characterize the film texture (similarly to that of the films deposited at 30−500 °C), a finer surface morphology is detectable, characterized by much smaller granular structures of homogeneous spherical shapes. Both features indicate an enhanced order of the film surface. In Figure 3c, the AFM analysis of the CHA film deposited at 750 °C is shown, it is clearly visible that the surface topography still resembles that discussed in Figure 3b.

The average surface roughness deduced from the AFM images is plotted in Figure 4, as a function of the deposition temperature, showing the significant roughness decrease (three times, from 62 to 18 nm) for the sample deposited at 700 °C. This result was reproduced upon several measurements so that a deeper analysis of the film deposited at 700 °C was required, and as such, high-resolution images were collected. In Figure 5, a 1 μm × 1 μm zoom is reported, where finer features of sample morphology are better evidenced: fine grain structure is clearly visible, together with some large agglomerates, characterizing the surface texture, still smooth as previously reported. The two line profiles, parallel to the horizontal line and passing through point 1 or point 2 in Figure 5, allowed us to estimate the fine grain dimension: 15−30 nm range of average grain height and 100−150 nm range of average lateral dimension.

The average grain height (15−30 nm) thus obtained is in good agreement with the grain size data obtained by the EDXRD technique. To estimate the grain size from a diffraction pattern, we used Laue equations to get the equivalent of the Scherrer formula (which applies to the angular dispersive case only) valid for energy-dispersive diffraction data analysis. The average grain size for the films deposited at 700 °C, obtained by analyzing the patterns making use of such modified Scherrer formula (the procedure is fully described in literature (40)), is about 25−40 nm, with this range being dependent on the analyzed reflection. The 25−40 nm range is in agreement with the grain size obtained by the AFM observation. Indeed, a more rigorous comparison should be made considering only the vertical dimension, obtained by the AFM measurements, because this technique is affected by a poor lateral resolution. These results are also in agreement with the SEM observations, reporting the presence on the film surface of micrometer-size droplets for the samples deposited in the range of 30−500 °C, and a finer granular surface morphology for the films deposited at 700 °C.

EDXRD measurements were performed to investigate the phase composition and structure of the deposited films. Prior to a systematic investigation of the films, the Ti substrate and the CHA target were examined. In the EDXRD patterns, all the Bragg peaks corresponding to titanium (hexagonal system, space group $P6_3/mmc$ (41)) are labeled in Figure 6a, whereas the attribution of the CHA crystalline reflections (hexagonal system, space group $P6_3/m$ (41)) is shown in Figure 6b. In the inset of Figure 6a, an AFM image, representative of the Ti substrate, is reported. The surface appears to be homogeneus and quite smooth, its roughness being about 7 nm. The AFM analysis of the CHA target was not possible, because the sample's roughness and the dimention of the granular domains are too high to be evaluated by this technique.

Figure 7 shows the diffraction patterns (shifted in intensity), collected in symmetrical diffraction geometry ($\alpha = 0°$), for films deposited at different substrate temperatures. The EDXRD patterns of the films deposited in the 30−500 °C range (empty dots) overlap perfectly, no CHA crystalline contribution being detectable despite the long counting time (7200 s). As already detected by SEM and AFM analyses, the 700 °C deposited film deserves special attention. The film appears to be crystalline, with several Bragg reflections being detected and assigned to CHA reflections and labeled in the graph as (1), (2), and (5): (1) (300) at $q = 2.34$ Å^{-1}, (2) (202) at $q = 2.38$ Å^{-1}, and (5) (212) at $q = 2.74$ Å^{-1}. Two further

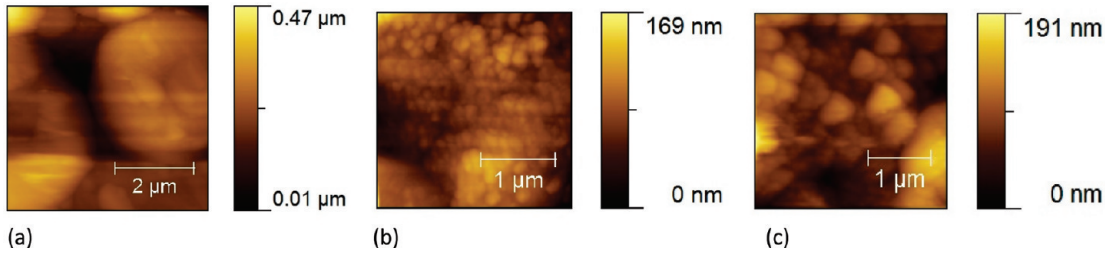

FIGURE 3. AFM images representative of surface morphology of film deposited at (a) 400 °C, image 5 μm × 5 μm; (b) 700 °C, image 3 μm × 3 μm; (c) 750 °C, image 3 μm × 3 μm.

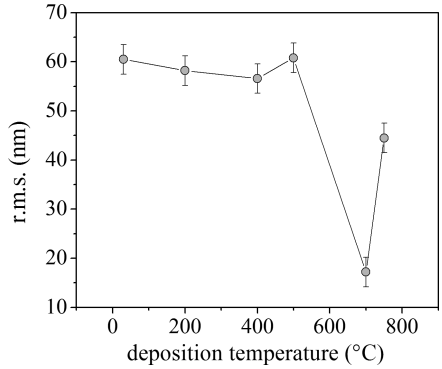

FIGURE 4. Surface roughness of CHA films, deduced from AFM measurements, as a function of deposition temperature.

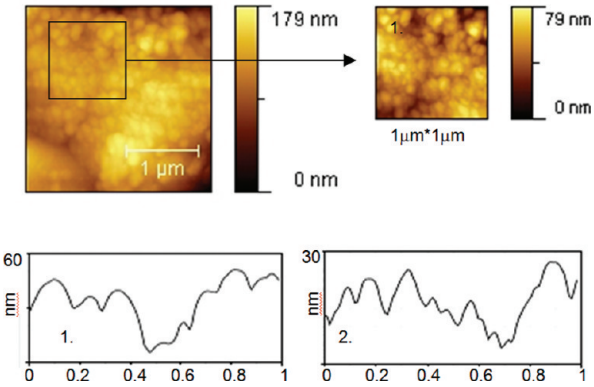

FIGURE 5. High-resolution AFM image of film deposited at 700 °C. Two profiles are shown to evidence the granular structure of the surface.

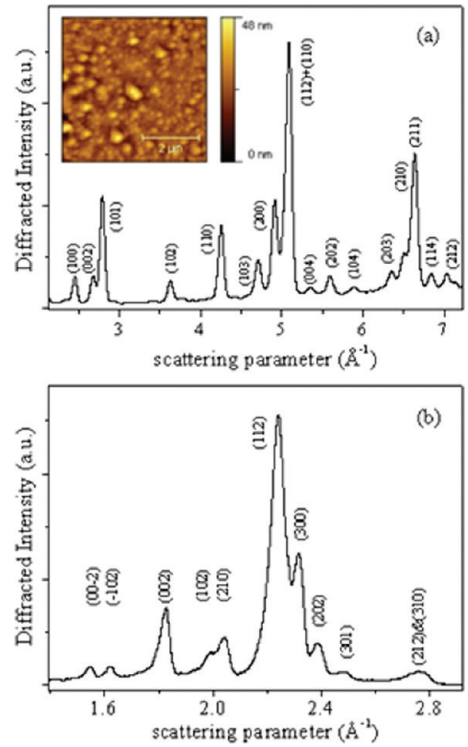

FIGURE 6. (a) EDXRD pattern collected as a function of the scattering parameter and (5 × 5) μm AFM image of Ti substrate. (b) EDXRD pattern of CHA target collected as a function of the scattering parameter. All crystalline reflections are labeled.

reflections, numbered (3) and (4), can univocally be attributed to the HA phase (hexagonal system, space group $P6_3/m$) (41)): (3) (152) at $q = 2.58$ Å^{-1} and (4) (125) at $q = 2.62$ Å^{-1}. The presence of other HA contributions can not be excluded, because their q-position coincides with that of the intense Ti substrate signals. Therefore, the results of the EDXRD measurements suggest that the 700 °C deposition temperature induces crystallization of the CHA material. Moreover, with the carbonate substitution into HA of 7.6 wt %, the peaks attibutable to the crystalline HA are registered as well. Finally, the pattern collected upon the 750 °C deposited film preserves some features of the 700 °C EDXRD spectra (peak 4, Figure 7).

To further investigate the structural properties of the crystalline film deposited at 700 °C, we performed EDXRD rocking curve analysis. The patterns collected at different asymmetry parameter values α are reported in Figure 8a. Tilting the sample, the intensity of the substrate reflections remains constant, whereas the various Bragg reflections of the film are enhanced. A detailed RC analysis revealed that the film shows preferential growth directions. The results are reported in Figure 8b. From the position of the two RC peaks, it turns out that the difference between the two orientations is of 0.52°. Furthermore, the analysis of the RC shapes indicates that the full width half maximum (fwhm) of the (202) reflection is 0.82°, whereas that of the (212) reflection is of 1.05°. These results indicate that the film is medium textured. In agreement, SEM and AFM techniques also evidence a smoother surface and more ordered texture for this samples.

In the case of film deposited at 750 °C, the HA (152) and (125) reflections are dominant, and characterized by a flat rocking curve, indicating partial decomposition of the CHA component, according to the FTIR results given below.

The FTIR spectra in the range of 2000−600 cm^{-1} of the pure Ti substrate and of CHA films samples deposited in the temperature range of 30−750 °C are shown in Figure 9. Absorption peaks are detected only in the films, being the

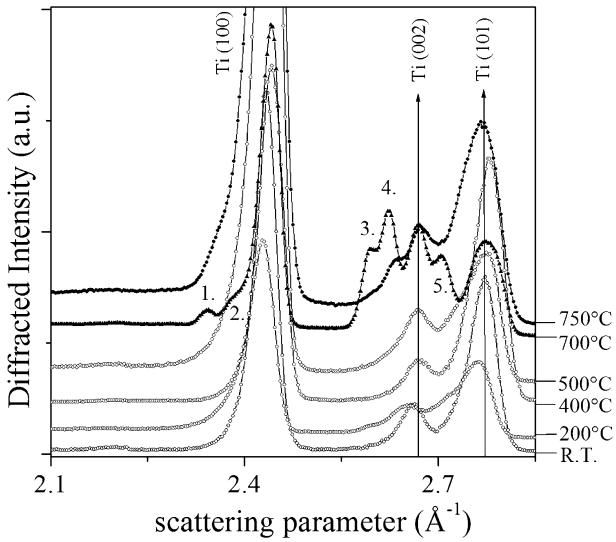

FIGURE 7. Sequence of EDXRD patterns collected from the films deposited at different temperatures. Empty dots are used to plot the patterns collected from the films deposited in the 30−500 °C range. Full triangles represent the 700 °C deposited film, the CHA/HA crystalline reflections are labeled from 1 to 5. Full dots represent the 750 °C deposited sample.

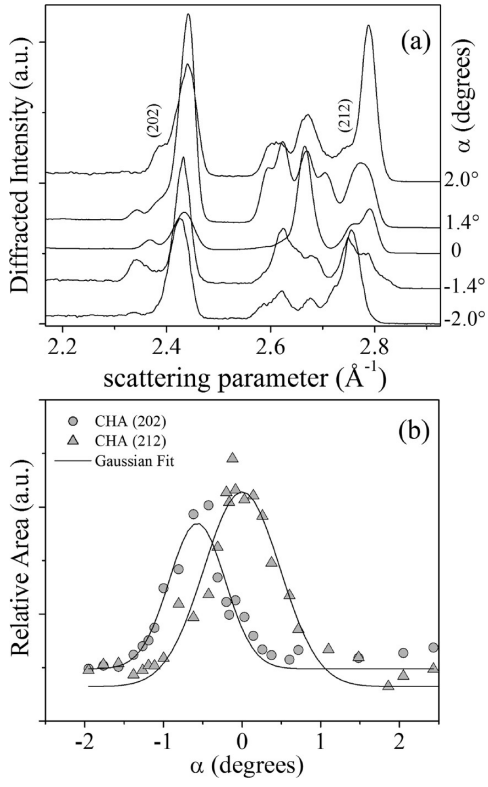

FIGURE 8. (a) EDXRD patterns collected upon film deposited at 700 °C film at different α values. (b) Rocking curves (dots) of CHA reflections and Gaussian fits (lines).

Ti substrate spectrum completely flat. The broad absorption of weak intensity at 1580 cm^{-1}, detected only at 30 and 200 °C, is attributed to the bending mode of the H_2O molecules. The stretching mode around 3300 cm^{-1}, not shown in Figure 9, supports such attribution. An additional feature at 1742 cm^{-1}, observed only at 30 °C, could probably be assigned to the CO group, coordinated by the calcium atoms of the deposit (42). Bands at 1397 and 996 cm^{-1}, present in the spectra for all deposition temperatures, were confidently assigned to the C−O and P−O double bonds of carbonate and phosphate components of the CHA molecule, respectively (43). In Figure 9, it is visible that for the 750 °C deposited film, the intensity of the band corresponding to the carbonate component (1397 cm^{-1}) is much diminished with respect to that of the 700 °C deposited sample (this is clearly confirmed by comparing the corresponding band areas). This experimental evidence corroborates the EDXRD results, both indicating that at the highest temperature a process of the CHA decomposition is present, in agreement with the literature data (44, 45).

To examine the mechanical properties of the films, Vickers microhardness measurements were carried out. First, the hardness of the CHA ceramic target was measured. The intrinsic hardness of the bulk target was found to be low, 2.7 ± 0.2 GPa, in correlation with hardness of pure HA sintered ceramics reported in literature, 4.6 ± 0.2 GPa (46). This is in agreement with the well-known poor mechanical properties (high brittleness) of calcium phosphates, which makes it impossible to use them in locations subjected to mechanical loads.

The roughness and irregularity of the film surface are considered to be an advantage for biomedical applications, providing better attachment of the osteoblast cells to the implant. However, the irregularity of a film results in a more complicated evaluation of both the film's thickness and hardness. The SEM images of Vickers pyramidal imprints on the film surface at different magnifications are shown in images a and b in Figure 10. It should be noted, however, that micrometer-size droplets present on the surface of the films deposited in the range of 30−500 °C did not influence much the hardness measurements, because the minimum average imprint diagonal (D), about 7 μm, turned out to be larger than the droplet diameter, 1−3 μm, even at low loads.

Calculated intrinsic hardness values for the CHA films on Ti substrates deposited at different temperatures are summarized in Table 1. As can be seen, the intrinsic hardness of films is rather low when the temperature of deposition is in the range of 30−500 °C. Conversely, at 700 °C the film is very hard, exhibiting 28 GPa hardness, which is much higher than that of the CHA bulk. The film deposited at 750 °C is still hard, although its hardness is lower than that of the film deposited at 700 °C. Likely, the enhanced hardness at 700 °C could be justified by a much lower film thickness (3.8 μm) with respect to thickness of films deposited at lower temperature (8−10 μm), but primarily by the crystalline textured nature of the film. This result and the data obtained by SEM, AFM, and EDXRD, indicating the formation at 700 °C of crystalline grains with nanometer size, are in full agreement with ref 47, in which it is reported that the transition to a nanocrystalline state is accompanied by an increase in hardness.

For comparison, the literature (48) on crystalline calcium phosphate coatings produced by PLD on Ti substrate shows a very low hardness of 1.6 GPa, for 1 μm thick coating. The hardness data we obtained in this work depositing at 700

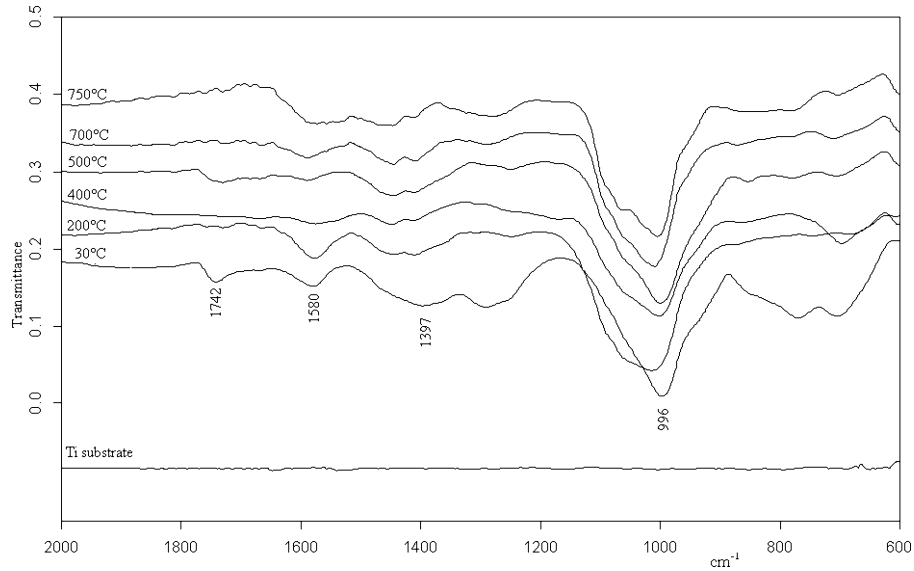

FIGURE 9. FTIR spectra of Ti substrate and CHA films on Ti substrates deposited in the range of 30−750 °C.

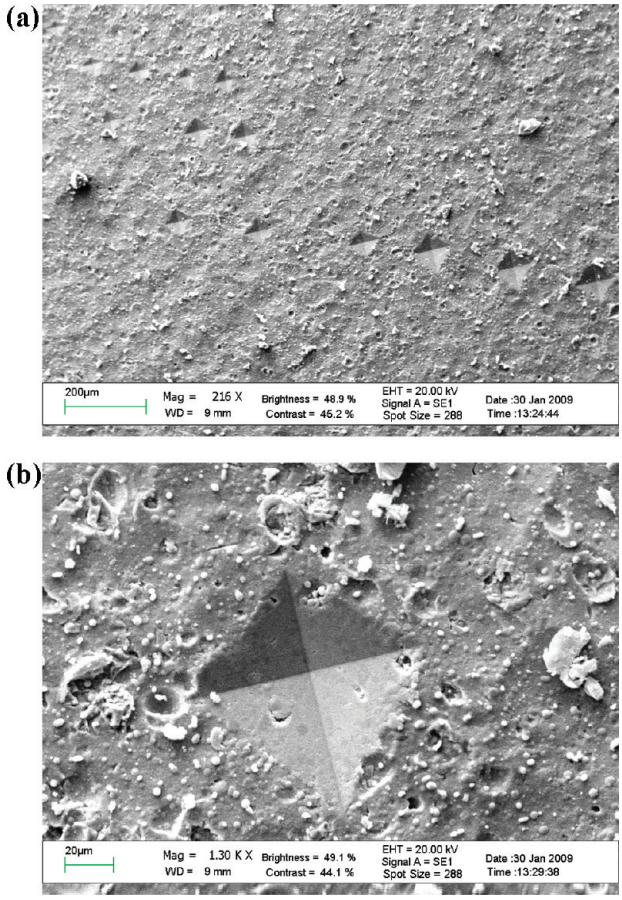

FIGURE 10. SEM micrographs of imprints on CHA film surface (deposited at 500 °C) at (a) 200 and (b) 1300 magnification.

°C are three times higher than other literature data (49), reporting 9 GPa of hardness for 3 μm thick calcium phosphate coatings on titanium deposited by rf-magnetron sputtering.

4. CONCLUSIONS

Carbonated hydroxyapatite films were obtained on titanium substrates by pulsed laser deposition method. The microscopical, spectroscopical, diffractometric, and Vickers microhardness techniques, applied for their characterization, provided complementary and fully consistent results, which can be summarized as follows.

The depositions in the 30−500 °C substrate temperature range led to the formation of about 9 μm thick amorphous films, characterized by large domains (500−600 nm of average height, 1−3 μm of average lateral dimension, 60 nm of average roughness). At higher deposition temperature (700 °C), 4 μm thick CHA films with a finer surface morphology (15−30 nm of average grain height, 100−150 nm of average lateral dimension, 20 nm of average roughness) were obtained. At this temperature, the films are crystalline, medium textured, and show privileged (202) and (212) orientations. The rocking curve fwhm is 0.82 and 1.05° for the (202) and the (212) reflections, respectively, with the mismatch between the two orientations being 0.52°.

The prepared films are nearly stoichiometric: the Ca/P atomic ratio is 1.81 for the films deposited at 30 °C, 2.10 for films deposited in the range of 200−700 °C, and 2.20 for films deposited at 750 °C.

CHA films are harder than the corresponding bulk material. Vickers hardness is 5−8 GPa for the 8−10 μm thick films on Ti substrates, deposited in the 30−500 °C temperature range. The films deposited at 700 °C show greatly improved mechanical properties. Indeed, the 4 μm thick films on Ti substrates are characterized by the hardness as high as 28 $\pm$ 3 GPa.

In conclusion, the present systematic investigation demonstrates that the PLD deposition performed at 700 °C allows to obtain CHA films fulfilling all the fundamental characteristics required for biomedical implant application. Indeed, the CHA materials must be thermally stable, so that it will not lose the carbonate groups substituted into the HA structure neither upon sintering procedure nor upon further heat treatment. Additionally, such films exhibit other important properties, such as good crystallinity, medium degree of texture, and elevated hardness.

REFERENCES AND NOTES

(1) Long, M.; Rack, H. J. *Biomaterials* **1998**, *19*, 1621.
(2) Ergun, C.; Doremus, R.; Lanford, W. *J. Biomed. Mater. Res., A* **2003**, *65*, 336.
(3) Feng, B.; Chen, J. Y.; Qi, S. K.; He, L.; Zhao, J. Z.; Zhang, X. D. *J. Mater. Sci. Mater. Med.* **2002**, *13*, 457.
(4) Ichinose, S.; Muneta, T.; Sekiya, I.; Itoh, S.; Aoki, H.; Tagami, M. *J. Mater. Sci. Mater. Med.* **2003**, *14*, 79.
(5) Lacefield, W. R. *Adv. Dent. Re.s* **1999**, *12*, 21.
(6) *Biological Performance of Biomaterials—Fundamentals of Biocompatibility,* 2nd ed.; Marcel Dekker: New York, 1993.
(7) Sun, L.; Berndt, C. C.; Gross, K. A.; Kucuk, A. *J. Biomed. Mater. Res., Part B* **2001**, *58*, 570.
(8) Yang, Y.; Kim, K. H.; Ong, J. L. *Biomaterials* **2005**, *26*, 327.
(9) Bigi, A.; Cojazzi, G.; Panzavolta, S.; Ripamonti, A; Roveri, N.; Romanello, M.; Noris Suarez, K.; Moro, L. *J. Inorg. Biochem.* **1997**, *68*, 45.
(10) Driessens, F. C. M. *Bull. Soc. Chim. Belg.* **1980**, *89*, 663.
(11) Mathew, M.; Takagi, S. J. *Res. Natl. Inst. Stand. Technol.* **2001**, *106*, 1035.
(12) Gibson, I. R.; Bonfield, W. *J. Biomed. Mater. Res.* **2002**, *59*, 697.
(13) Martinetti, R.; Harmand, M. F.; Dolcini, L. *Key Eng. Mater.* **2004**, *233*, 254–256.
(14) Porter, A.; Patel, N.; Brooks, R.; Best, S.; Rushton, N.; Bonfield, W. *J. Mater. Sci.: Mater. Med.* **2005**, *16*, 899.
(15) Hankermeuer, C. R.; Ohashi, L. L.; Delaney, D. C.; Ross, J.; Constantz, B. R. *Biomaterials* **2002**, *23* (3), 743.
(16) Chang, E.; Chang, W. J.; Wang, B. C.; Yang, C. Y. *J. Mater. Sci.: Mater. Med.* **1997**, *8*, 193.
(17) Kurzweg, H.; Heimann, R. B.; Troczynski, T. *J. Mater. Sci.: Mater. Med.* **1998**, *9*, 9.
(18) Balamurugan, A.; Kannan, S.; Rajeswari, S. *Trends Biomater. Artif. Organs* **2002**, *16*, 18.
(19) Cui, F. Z.; Luo, Z. S.; Feng, Q. L. *J. Mater. Sci.: Mater. Med.* **1997**, *8*, 403.
(20) Takahashi, K.; Hayakawa, T.; Yoshinari, M.; Hara, H.; Mochizuki, C.; Sato, M.; Nemoto, K. *Thin Solid Films* **2005**, *484* (1—2), 1.
(21) Cleries, L.; Fernandez-Pradas, J. M.; Sardin, G.; Morenza, J. L. *Biomaterials* **1998**, *19*, 1483.
(22) Ball, M. D.; Downes, S.; Scotchford, C. A.; Antonov, E. N.; Bagratashvili, V. N.; Popov, V. K.; Lo, W. J.; Grant, D. M.; Howdle, S. M. *Biomaterials* **2001**, *22*, 337.
(23) Gyoergy, E.; Toricelli, P.; Socol, G.; Iliescu, M.; Mayer, I.; Mihailescu, I. N.; Bigi, A.; Werckman, J. *J. Biomed. Mater. Res., Part A* **2004**, *71* (2), 353.
(24) Bigi, A.; Bracci, B.; Cuisinier, F.; Elkaim, R.; Fini, M.; Mayer, I.; Mihailescu, I. N.; Socol, G.; Sturba, L.; Torricelli, P. *Biomaterials* **2005**, *26* (15), 2381.
(25) Bao, Q.; Chen, C.; Wang, D.; Ji, Q.; Lei, T. *Appl. Surf. Sci.* **2005**, *252* (5), 1538.
(26) Mihailescu, I. N.; Torricelli, P.; Bigi, A.; Mayer, I.; Iliescu, M.; Werckmann, J.; Socol, G.; Miroiu, F.; Cuisinier, F.; Elkaim, R.; Hildebrand, G. *Appl. Surf. Sci.* **2005**, *248* (1—4), 344.
(27) Solla, E. L.; Borrajo, J. P.; Gonzalez, P.; Serra, J.; Chiussi, S.; Leon, B.; Lopez, J. G. *Appl. Surf. Sci.* **2007**, *253* (19), 8282.
(28) Bao, Q.; Chen, C.; Wang, D.; Liu, J. *Cryst. Growth Des.* **2008**, *8* (1), 219.
(29) Cricenti, A.; Generosi, R. *Rev. Sci. Instrum.* **1995**, *66* (4), 2843.
(30) Felici, R.; Cilloco, F.; Caminiti, R.; Sadun, C.; Rossi, V. Italian Patent No. RM 93 A 000410, 1993.
(31) Paci, B.; Generosi, A.; Rossi Albertini, V.; Agostinelli, E.; Varvaro, G.; Fiorani, D. *Chem. Mater.* **2004**, *16*, 292.
(32) Ferro, D.; Scandurra, R.; Latini, A.; Rau, J. V.; Barinov, S. M. *J. Mater. Sci.* **2004**, *39* (1), 329.
(33) Ferro, D.; Rau, J. V.; Rossi Albertini, V.; Generosi, A.; Teghil, R. *Surf. Coat. Technol.* **2008**, *202* (8), 1455.
(34) Joensson, B.; Hogmark, S. *Thin Solid Films* **1984**, *114* (3), 257.
(35) Iost, A.; Bigot, R. *Surf. Coat. Technol.* **1996**, *80* (1—2), 117.
(36) Froehlich, F.; Grau, P.; Grellman, W. *Phys. Status Solidi A* **1977**, *42* (1), 79.
(37) Korsunsky, A. M.; McGurk, M. R.; Bull, S. J.; Page, T. F. *Surf. Coat. Technol.* **1998**, *99* (1—2), 171.
(38) Puchi-Cabrera, E. S. *Surf. Coat. Technol.* **2002**, *160* (2—3), 177.
(39) Brunette, D. M.; Tengvall, P.; Textor, M.; Thomsen, P., Eds. *Titanium in Medicine*; Springer: Berlin, 2001.
(40) Rau, J. V.; Ferro, D.; Falcone, M. B.; Generosi, A.; Rossi Albertini, V.; Latini, A.; Teghil, R. *Mater. Chem. Phys.* **2008**, *112*, 504.
(41) International Centre for Diffraction Data, Database JCPDS, 2000.
(42) Hauge, R. H.; Gransden, S. G.; Margrave, J. L. *Proc. Electrochem. Soc.* **1978**, *78* (1), 310.
(43) Rau, J. V.; Nunziante Cesaro, S.; Ferro, D.; Barinov, S. M.; Fadeeva, I. V. *J. Biomed. Mater. Res.* **2004**, *71B*, 441.
(44) Barralet, J.; Knowles, J. C.; Best, S.; Bonfield, W. *J. Mater. Sci. Mater. Med.* **2002**, *13*, 529.
(45) Barinov, S. M.; Bibikov, V.Yu.; Fadeeva, I. V.; Ferro, D.; Komlev, V. S.; Medvecky, L.; Nunziante Cesaro, S.; Rau, J. V. *Powder Met. Prog.* **2004**, *4* (2), 95.
(46) Ferro, D.; Barinov, S. M.; Rau, J. V.; Teghil, R.; Latini, A. *Biomaterials* **2005**, *26*, 805.
(47) Andrievski, R. A. *Int. J. Refract. Met. Hard Mater.* **2001**, *19*, 447.
(48) Arias, J. L.; Mayor, M. B.; Pou, J.; Leng, Y.; Leon, B.; Perez-Amor, M. *Biomaterials* **2003**, *24*, 3403.
(49) Pichugin, V. F.; Surmenev, R. A.; Shesterikov, E. V.; Ryabtseva, M. A.; Eshenko, E. V.; Tverdokhlebov, S. I.; Prymak, O.; Epple, M *Surf. Coat. Technol.* **2008**, *202*, 3913.

AM900356E